The Journal of Experimental Biology 215, 3639-3648

doi:10.1242/jeb.075416

RESEARCH ARTICLE

Locomotion analysis identifies roles of mechanosensory neurons in governing locomotion dynamics of *C. elegans*

Emiliano Cohen[1], Eviatar Yemini[2], William Schafer[2], Dror G. Feitelson[3] and Millet Treinin[1,*]

[1]Department of Medical Neurobiology, Hebrew University – Hadassah Medical School, Jerusalem 91120, Israel, [2]Cell Biology Division, MRC Laboratory of Molecular Biology, Hills Road, Cambridge CB2 0QH, UK and [3]Department of Computer Science, Hebrew University, Jerusalem 91904, Israel

*Author for correspondence (millet_t@cc.huji.ac.il)

SUMMARY

The simple and well-characterized nervous system of *C. elegans* facilitates the analysis of mechanisms controlling behavior. Locomotion is a major behavioral output governed by multiple external and internal signals. Here, we examined the roles of low- and high-threshold mechanosensors in locomotion, using high-resolution and detailed analysis of locomotion and its dynamics. This analysis revealed a new role for touch receptor neurons in suppressing an intrinsic direction bias of locomotion. We also examined the response to noxious mechanical stimuli, which was found to involve several locomotion properties and to last several minutes. Effects on different locomotion properties have different half-lives and depend on different, partly overlapping sets of sensory neurons. PVD and FLP, high-threshold mechanosensors, play a major role in some of these responses. Overall, our results demonstrate the power of detailed, prolonged and high-resolution analysis of locomotion and locomotion dynamics in enabling better understanding of gene and neuron function.

Key words: *Caenorhabditis elegans*, locomotion, mechanosensation.

Received 28 May 2012; Accepted 5 July 2012

INTRODUCTION

To survive in an ever-changing environment, metazoans have evolved complex neuronal networks. Neurons sense, integrate and transmit information to finally produce complex adaptive behaviors. *Caenorhabditis elegans*, having a simple and well-characterized nervous system of only 302 neurons, is an excellent model for understanding the roles of specific molecules and neurons in nervous system function (White et al., 1986). The major behavioral output of the *C. elegans* nervous system is locomotion. Locomotion enables escape from noxious stimuli or navigation towards positive signals such as food. *Caenorhabditis elegans* navigates its environment by propagating a sinusoidal waveform that is generated by a well-defined motor circuit (Von Stetina et al., 2006). Information perceived by sensory neurons governs this motor circuit to control reversals (tail-first movement), speed, pauses and turns (Croll, 1975; Gray et al., 2005; Tsalik and Hobert, 2003; Wakabayashi et al., 2004; Zhao et al., 2003).

As *C. elegans* is a soil-dwelling nematode, its locomotion is likely to be strongly affected by collisions with soil particles. Indeed, analysis of *C. elegans* behavior identified several sets of mechanosensory neurons whose activation strongly affects locomotion (Chalfie and Sulston, 1981; Kaplan and Horvitz, 1993; Li et al., 2011). We have previously analyzed locomotion of strains defective for mechanosensation (Albeg et al., 2011). This analysis showed that the PVD and FLP high-threshold mechanosensors affect locomotion, and suggested that they activate an escape response. We note that this analysis was performed in the absence of acute sensory stimulation; thus, the identity of the stimulus activating this escape response remained unknown (Albeg et al., 2011).

Here, we used a tool kit that combines improved single-worm tracking and image analysis software to enable detailed analysis of multiple locomotion properties and their dynamics. The aim of this tool kit is to provide a comprehensive and detailed characterization of the function of neurons and genes in controlling behavior. For this we have modified and enhanced the image and locomotion analysis previously used by Albeg et al. (Albeg et al., 2011). The current software uses images and data provided by a 'worm-tracker' unit for higher resolution and prolonged tracking of single animals. Using this tool kit, we analyzed previously characterized strains (Albeg et al., 2011). Our results reveal novel roles for mechanosensory neurons in regulating locomotion. They also demonstrate long-lasting (minutes) effects of noxious mechanical stimuli on locomotion, showing that these long-lasting effects entail changes in multiple locomotion properties. Importantly, our work shows different half-lives of effects on different locomotion properties, and suggests that different locomotion properties are controlled by different partly overlapping sets of neurons. Overall, our results demonstrate the power of detailed locomotion analysis in revealing novel functions of genes and neurons.

MATERIALS AND METHODS

Animals and assay conditions

Strains used in this study are described elsewhere (Albeg et al., 2011). Briefly, the *mec-4(e1611)* mutation leads to degeneration of the six touch receptor neurons (ALMs, PLMs, AVM and PVM; –T animals), the integrated *ser-2prom3::deg-3(N293I)* transgene eliminates, *via* degeneration, PVDs (–P animals), the integrated *mec10p::deg-3(N293I)* transgene eliminates, *via* degeneration, 10 body mechanosensors (six touch receptor neurons, FLPs and PVDs),

and *mec-10(tm1552)* is a *mec-10 loss of function* [*mec-10(lf)*] mutation. Animals were grown at 20°C on standard nematode growth media (NGM) plates seeded with the *E. coli* strain OP50. For each assay, L4 animals were picked for overnight growth on fresh NGM plates. At the start of each experiment a single animal was transferred with a wire pick to a fresh newly seeded NGM plate and worm tracking was initiated at the moment that the animal's image was captured, up to half a minute following transfer. All movies analyzed here track the animals for 20 min. Bacterial lawns on plates used for image analysis were allowed to grow to a thin regular layer surrounded with a clear unseeded border to limit wandering of animals to the edge of the plate and to enable better image identification and longer tracking.

Worm-tracking hardware

A description of the Worm Tracker 2.0 hardware enabling image acquisition and centering of the nematode's image as it moves on an agar plate can be found at http://www.mrc-lmb.cam.ac.uk/wormtracker/index.php?action=hardware.

Worm-tracking software

Worm Tracker 2.0 software enabling identification of the animal and centering of the microscope camera on this animal as it moves is described in http://www.mrc-lmb.cam.ac.uk/wormtracker/ and is freely available from this site. This software is compatible with all Windows operating systems from XP to Windows 7. All Ludl, Prior and Zaber brand motorized stages are supported. All cameras with DirectShow filters (the majority of USB cameras) are supported. The software provides automatic calibration for directing the stage and converting the pixel coordinates, in its recorded movies, to real-world micrometers. Several other options allow the software to be configured for specialized applications, such as those requiring tracking of light objects on a dark background or using corrective manual movements (e.g. employing a joystick) in conjunction with automated tracking to follow extremely fast objects. A guide on the website provides further instructions for software configuration and use.

Image and movement analysis

The software used for image analysis is based on software described previously (Albeg et al., 2011), and, specifically, the calculation of posture and movement parameters remains as described there. This software was adapted for movies generated by the worm-tracking module described above and utilizes the information on stage movement provided by this module to identify the relative locations of the movie frames. It is written in VisualC++ and utilizes the openCV image analysis library provided by Intel, leading to an analysis rate that is about twice real time (analyzing a 20 min movie at 10 frames s^{-1} takes around 10 min). The main algorithms used are as follows.

Binarization

For each frame, a gray-level histogram is generated. The largest maximum in the histogram represents the background. The nearest minimum below this maximum is used as a threshold for binarization. This is combined with edge detection to improve identification of the nose and tail. Holes are closed using dilation followed by erosion. Connected-components analysis is used to identify the largest connected component and discard smaller ones.

Skeletonization

First, a distance map is generated for the binary silhouette of the worm, and the maximum found. Using the maximum as a starting point, a walk is performed along the main ridge of the distance map in both directions. This is done by drawing a semi-circle with radius 4 pixels around the current point in the direction opposite to the previous point, finding the maximal point on this semi-circle, and connecting to it by an 8-neighbor line. Looping back at the end is prevented by disallowing two sharp turns in a row.

Loop identification

Loops are identified when the skeleton touches or crosses itself. A possible problem is that the hole in the middle of a loop may have been closed in the binarization phase. This is corrected by calculating a distance map and, if the maximum is more than 80% the average width of the worm, checking whether the location of the maximum was actually part of the background in the original image.

Head identification

The head is identified as being brighter than the tail. Specifically, the gray-level histogram for a 1/10 mm segment at each end of the worm is calculated. The brightness is then defined to be the average gray level of the brightest 20% of the pixels. If the average at one end is higher (lighter) by 2 or more it is identified as the head. All consecutive frames in between problem frames (e.g. loops) are grouped together. In each such group, frames with consistent head orientation are identified based on distances between locations in successive frames. The correct orientation is then identified using majority vote. Manual inspection shows that this method is reliable except for movie segments in which the animal pauses in close proximity to its newly laid eggs, as the space between the worm and the egg is typically light. Such errors occur primarily during pause segments and thus have no effect on the correct identification of locomotion patterns (i.e. forward *versus* backward movement). In contrast to the previous version of the software, the head identification is now completely automated requiring no manual verification.

Executable, source code, sample inputs and outputs and a manual are available at http://www.cs.huji.ac.il/~feit/worms/.

Data and statistical analysis

Data were analyzed using standard Matlab algorithms. Data were fitted to equations using the fit function (http://www.mathworks.com/help/toolbox/curvefit/fit.html), specifically the NonlinearLeastSquares method (LinearLeastSquare method was used when fitting to linear equations). Optimal fit (R^2) was achieved *via* iteration of the analysis 100 times and choosing values having the highest R^2. The Trust-Region algorithm was used to calculate 95% confidence intervals.

RESULTS

The tool kit

Analysis is carried out on a single worm moving on an agar plate. The animal is positioned above an integrated microscope camera that is connected to a computer. Tracking initiates once the animal is found within the camera's frame. To track the animal, the system controls the camera's position using a motorized stage. Only the camera moves – the worm's platform is kept motionless so as not to disrupt the animal's behavior. This tracking system produces three outputs: a movie of the animal, information on stage movements, and information on camera and stage calibrations. The first two outputs are used as inputs to the image analysis software (Fig. 1).

The image analysis software starts by identifying the animal using thresholding and edge detection to create a binary image of the animal. This is followed by skeleton identification and head assignment. Binarization and skeletonization are done on each frame

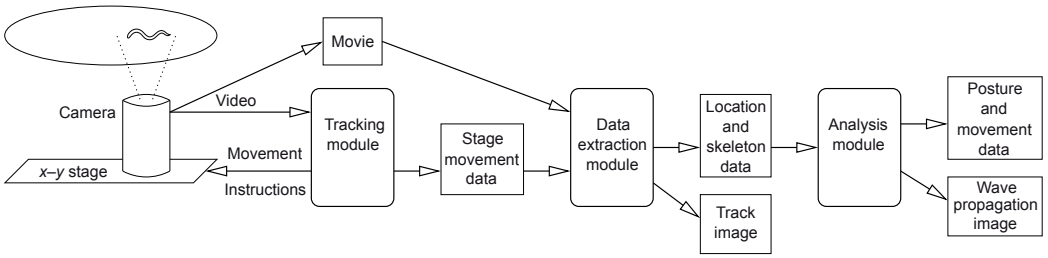

Fig. 1. Schematic diagram of the tool kit. Hardware is on the left and software modules are on right. The tracking, data extraction and analysis modules are implemented in software. In the current implementation the data extraction and analysis are bundled together.

separately; head assignment also uses information from surrounding frames and information on position of the worm derived from both the movie and the stage movement outputs. Frames in which the skeleton is ill formed (as in a loop) or its length deviates by more than 9% from the median are considered inconsistent and discarded from the analysis. The skeleton and head assignment for each frame combined with the information on stage movements are used for classifying each frame into a locomotion pattern (forward movement, backward movement, pause, omega or loop) (Albeg et al., 2011). The position of the skeleton's mid-point from each frame and information on stage movements are used for speed and displacement analysis. The skeleton is also used for analysis of postural properties. A short description of the outputs generated by this analysis program is provided in Table 1. Output files are in CSV format enabling further analysis using Matlab or Excel.

Characterization of locomotion patterns

The wild-type *C. elegans* (N2) lies on its side generating an anterior to posterior propagating sinusoidal waveform in order to move forward (head first). This forward locomotion is interspersed with reversals (backward movement), pauses and loops that in some cases lead to an altered direction of movement (Croll, 1975). Sensory cues are known to control the frequency and duration of these locomotion patterns (Croll, 1975; Gray et al., 2005; Tsalik and Hobert, 2003; Wakabayashi et al., 2004; Zhao et al., 2003). Thus, several 'movement analysis' programs classify locomotion into forward, backward, pause and loops (curls) (Albeg et al., 2011; Geng et al., 2004; Hoshi and Shingai, 2006). We slightly modified this classification by separately analyzing omegas (animals showing an exaggerated body bend) (Albeg et al., 2011) and loops (animals whose skeleton forms a closed loop). Loops pose a problem for analysis, as characterization of the skeleton and head identification in this configuration are not possible using our current software. However, identification of this postural configuration is important as it is often associated with direction changes. Using this classification method we show that in N2 animals the reversal frequency (initiation of backward movement) is $3.9\pm0.34\,\text{min}^{-1}$ and the average duration of backwards movement is 0.69 s. Similarly, pauses are $13\pm0.81\,\text{min}^{-1}$ and last on average 1.19 s. Both omegas and loops are rarely seen in N2, with a frequency of 0.3 ± 0.09 and $0.19\pm0.05\,\text{min}^{-1}$, respectively. These numbers represent averages for 14 animals during 20 min movies. We note that the high variability of these numbers is a result of the dynamic nature of locomotion, as both frequency and duration of each locomotion pattern are regulated by multiple signals including time from transfer to a new plate. For example, both the frequency and duration of backward movement increase with time from the start of analysis (see below).

An important feature of our software is that locomotion and posture properties such as speed, bending angle and bend amplitude are analyzed separately for different locomotion patterns. This distinction between locomotion patterns is unique to this tool kit, and was first introduced in a previous study (Albeg et al., 2011). This feature is important in order to reduce confounding effects such as the effects of including pauses in analyses of speed or of including omegas and loops in analyses of bending angle. Such confounding effects will increase variability and thus reduce sensitivity to small phenotypic differences when comparing mutant strains. In addition, averaging locomotion properties from all locomotion patterns may confound effects on frequency or duration of locomotion patterns with effects on speed or posture.

For a graphical illustration of the major postural properties measured by this program see Fig. 2A. Bend angle, normalized bend amplitude and cut-point number are analyzed for each frame in which a consistent skeleton is identified, while normalized wavelength is only calculated for skeletons having a posture with sufficient wave-like features (Albeg et al., 2011). Analysis of these properties in N2 (Fig. 2) demonstrates significant differences in posture between locomotion patterns not defined by posture (omegas and loops are defined by posture while forward and backward movement and pauses are not). This analysis shows that cut point number, bend angle and bend amplitude differ between backward and forward movement, while the posture of animals during pauses is similar to that seen during backward movement. The clear differences between forward and backward locomotion and the low variation of the results provide strong and unbiased support for our software's ability to correctly classify locomotion patterns. Differences in posture between forward and backward movement are associated with differences in speed: speed is higher for forward movement (Fig. 2B). Importantly, these results are consistent with previous results showing that backward movement is characterized

Table 1. Outputs generated by the data extraction and analysis modules

Output file	Description
wxo	Distributions of posture parameters for the whole movie and separately for each locomotion pattern
wxd	Full frame-by-frame dump of measured posture parameters
wxs	Distribution and statistics of locomotion patterns
spd	Speed of movement per frame and per 0.5 s segment
dsp	Displacement in successive 0.5 s segments
ang	Changes in angle of movement in successive 10 s segments
track	Composite image of worm's track throughout the movie
wave	Map of wave propagation along the worm's skeleton
skel	Full listing of skeleton points in each frame for future analysis

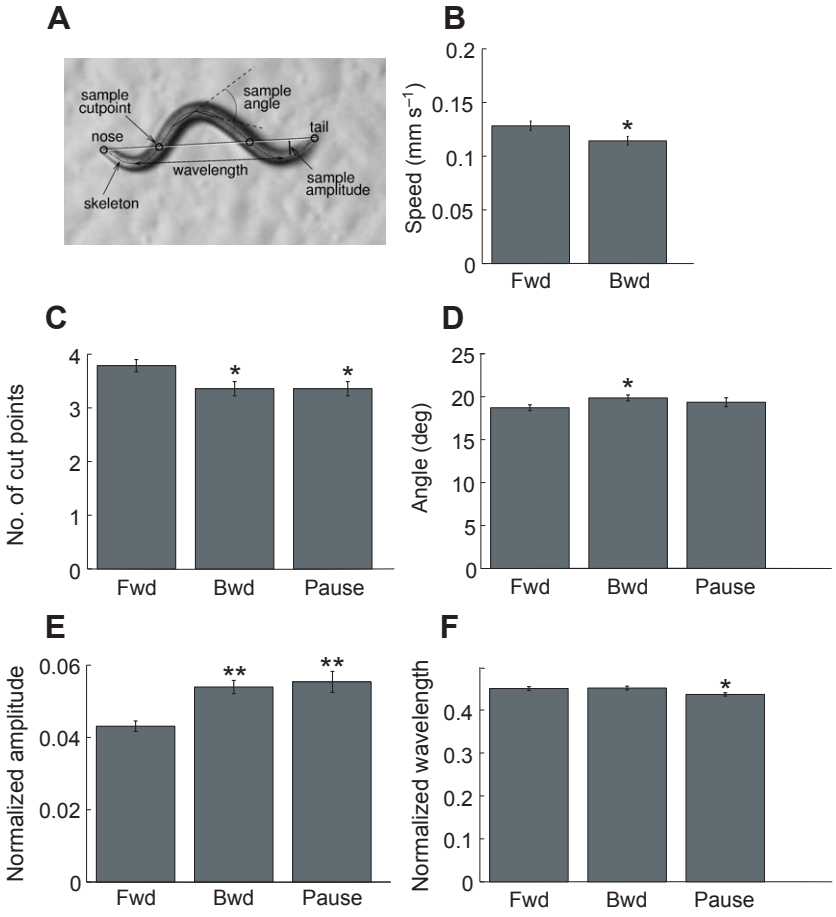

Fig. 2. Properties of locomotion patterns. (A) Diagramatic representation of parameters used for postural analysis. Circles surround cut-points between the animal's skeleton and a straight line connecting the head and tail. (B) Average speed. (C) Average cut-point number. (D) Average bending angle. (E) Average normalized amplitude. (F) Average normalized wavelength. Each number represents the average from 14 N2 animals classified as forward (Fwd), backward (Bwd) or pause. Numbers in C–F represent averages of the median result of all frames classified as above. Asterisks indicate significant difference relative to forward movement (*P<0.05, **P<0.01, t-test).

by increased bending amplitude and angle (Croll, 1975; Gray et al., 2005). In addition, similarity in normalized wavelength between forward and backward movement also reproduces previous results (Fig. 2F) (Cronin et al., 2005). Last, our current high-resolution analysis provides a sensitive method for posture analysis, showing that elimination of PVD neurons leads to a significant (P<0.01) increase in normalized wavelength (0.5±0.005 relative to 0.45±0.005 during forward movement in animals lacking PVD relative to N2; N=10 and N=14, respectively). We have previously suggested that elimination of PVD leads to increased wavelength, but those previous results suffered from high variability and the differences were not significant (Albeg et al., 2011). We believe that the increased resolution afforded by the worm-tracking unit has reduced inaccuracies, enabling increased sensitivity of this analysis.

Visualization tools reveal phenotypic differences in the dynamics of locomotion

To facilitate identification of new locomotion phenotypes our software provides two visualization tools: detailed traces of the animal's locomotion and images of wave propagation (Figs 3, 4). Both tools provide visual representations for locomotion dynamics and allow for unbiased inspection by the sensitive human eye for altered locomotion patterns.

The first tool shows superimposed images of the animal as it traverses the plate. In these images gray scale is used to indicate the time spent at each location, with light gray indicating short time duration (i.e. high speed) and black indicating prolonged duration (i.e. pause) (Fig. 3). This tool is a modified version of a tool presented in previous work (Albeg et al., 2011). The second tool is also an adaptation from previous work (Korta et al., 2007). In the resulting images the x-axis is time and the y-axis is position along the animal's skeleton. The gray scale indicates bending angle, with white indicating maximal bend in one direction and black indicating maximal bend in the other. The resulting diagonal lines depict propagation of body bends over time. The density of these lines and their slopes indicate speed and movement direction, respectively (top is head and thus diagonals sloping down to the right indicate forward movement). In these images, consistent forward movement results in regularly spaced diagonal lines, reversals are associated with a zigzag pattern (segments of backward movement are shorter than those of forward movement) (Croll, 1975), and pauses with horizontal smears (Fig. 4).

Using the first tool, we traced movement of N2 and of strains lacking specific mechanosensory neurons (Albeg et al., 2011). Traces of N2 beginning immediately after transfer to an agar plate seeded with bacteria reproducibly show animals starting with a roaming-type locomotion, with high speed and few if any directional changes [escape or dispersal have also been used as terms to describe similar locomotion patterns (Gray et al., 2005; Wakabayashi et al., 2004; Zhao et al., 2003)]. As time progresses these animals shift to a dwelling-type movement typified by increased pauses and directional changes (Fig. 3A). Similarly, others have shown that transfer with a wire pick leads to a transient inhibition of reversals that depends on body mechanosensors (Zhao et al., 2003). Indeed, traces showing movement of animals lacking all body mechanosensors [touch receptor neurons, PVDs and FLPs; –TPF animals (Albeg et al., 2011); Fig. 3B] support involvement of body mechanosensors in generating this dynamic behavior following

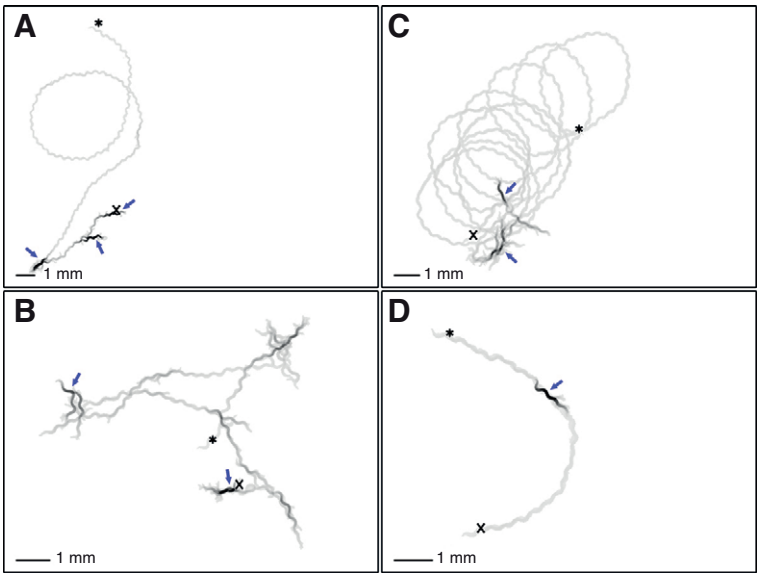

Fig. 3. Traces of *C. elegans* locomotion. (A) Wild-type. (B) Animals lacking body mechanosensors (–TPF). (C) Animals lacking touch receptor neurons (–T). (D) Quiescent pause. Light gray indicates short time duration (i.e. high speed) and black indicates prolonged duration (i.e. pause). Arrows in A–D indicate strong pauses. Asterisks indicate the start of the track; crosses indicate the end of the track.

transfer to a new plate. Further visual evidence for this shift from roaming to dwelling is provided by bend propagation images (Fig. 4A compared with 4E, first and last minute of a repesentative movie, respectively). These changes in locomotion properties are quantified in detail below. Interestingly, the dynamics of this behavior are opposite to what is seen in the absence of food: upon transfer to an unseeded plate animals start by initiating local search behavior (similar to dwelling) and with time shift to dispersal-promoting behavior (roaming) (Gray et al., 2005; Hoshi and Shingai, 2006).

Traces of –T animals lacking low-threshold body mechanosensors [in *mec-4(e1611)* animals, all six touch receptor neurons degenerate (Driscoll and Chalfie, 1991)] show circular tracks suggesting a bias in movement direction (Fig. 3C). In 13 traces, 10 show more than one full circle. Interestingly, similar bias, although much weaker, is sometimes seen in tracks of N2 (Croll, 1975; Stephens et al., 2010; Zhao et al., 2003). To quantify this bias we analyzed curvature of the track in N2 relative to that of –T mutants (Ben Arous et al., 2009). For this analysis curvature was only measured during segments of rapid forward movement in order to avoid the confounding effects of high curvatures measured following reversals or loops. Analysis of curvature angles over time for individual animals showed that while the track of a single N2 usually contains both negative and positive curve angles (Fig. 5A), tracks of –T animals have higher curve angles that are mostly positive or mostly negative (Fig. 5B compared with 5C). The average of the track curvatures for –T animals is 25.9±4.06 deg compared with 12.6±1.2 deg for N2 (N=13 and 14, respectively). Because the average track curvature for individual animals is either negative or positive, we averaged the absolute values of these averages. Careful examination of changes in track curvature over time (Fig. 5A–C) suggests that it may decay with time. To better examine this observation we averaged absolute curvature angle for all N2 or –T animals in successive 1 min segments. This analysis showed that track curvature angle decays over the first 5 min of the analysis (Fig. 5D). Indeed, data on track curvature fit well with a power

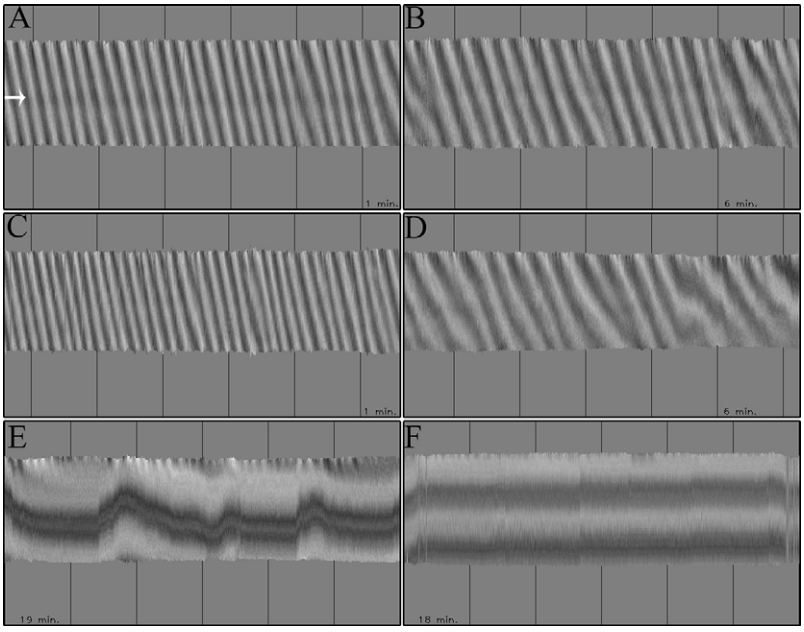

Fig. 4. Body-bend propagation images. (A) N2, first minute, roaming. (B) N2, 5th–6th minute, reduced speed. (C) –T, first minute. (D) –T, 5th–6th minute, showing irregular speed. (E) N2, last minute (19th), dwelling. (F) N2, quiescent pause. Time from the beginning of the analysis is indicated at the bottom. Lines indicate 100 frame intervals (10 s).

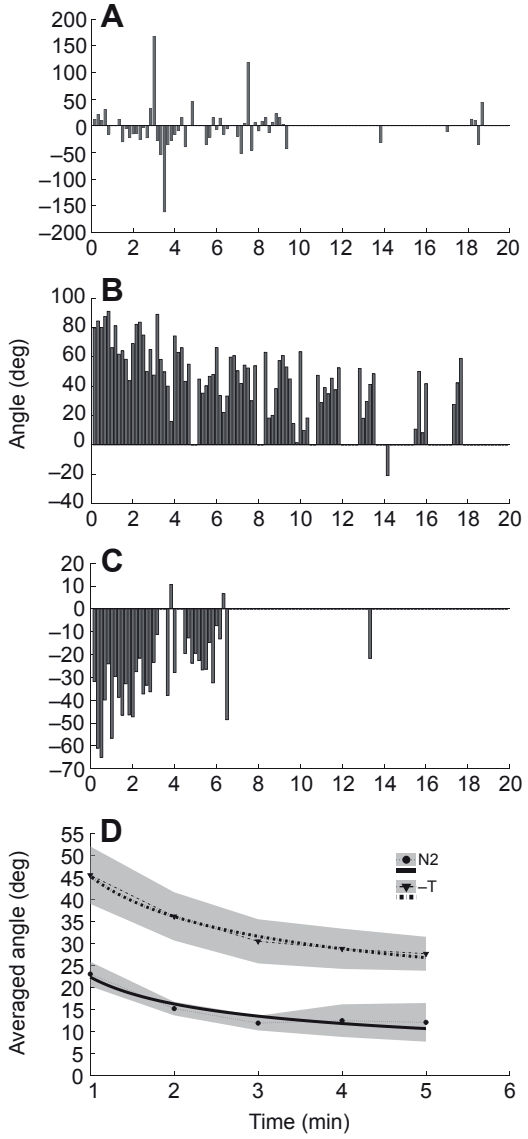

Fig. 5. Track curvature in N2 compared with –T animals. (A) Curvature angles over time for a representative N2 animal. (B,C) Curvature angles over time for two representative –T animals. In B, curvature is mostly positive and in C it is mostly negative. Positive is clockwise or to the right, and negative is counterclockwise or to the left. (D) Average curvature angles over time for N2 and –T (N=14 and N=13, respectively). Curvature angles were averaged over 1 min time segments to reduce noise. Standard error interval is shaded. Data are fitted with a power function $f(x)=ax^b$, with the following values: a=22.39, 45.35 confidence interval 17.97:26.81, 42.84:47.86; b=–0.46, –0.32 confidence interval –0.68:–0.23, –0.38:–0.26; R^2=0.92, 0.99 for N2 and –T, respectively.

function having a negative exponent. Only the first 5 min were analyzed as at later times curvature angles become highly variable or cannot be measured because of frequent reversals. We conclude that track curvature is controlled by touch receptor neurons and external stimuli, likely to be the noxious mechanical stimuli inflicted on the animal as it is being transferred to the plate used for analysis.

To further examine this curve angle preference we used egg-laying events to identify the ventral side of each animal (the vulva is on the ventral side and as animals lie on either their left or right side, the orientation of the ventral side in individual animals needs to be examined). This analysis shows that in all nine –T animals for which the ventral side could be identified, tracks always curved towards the ventral side. N2, while showing smaller average curve angles, also show some bias (i.e. negative or positive average curvature). Analysis of these animals showed that in 10 of 14 animals the tracks curved towards the ventral side. Based on this analysis we suggest that *C. elegans* have an intrinsic ventral curve angle bias during forward movement, a bias that is normally suppressed by touch receptor neurons. Previous work suggested that asymmetric innervation of head muscles leads to ventral direction bias following reversals (Gray et al., 2005). This asymmetry may also underlie the bias seen here for forward movement.

The phenotypes demonstrated above can be quantified using standard indicators. However, visualization tools also enable subclassification of locomotion patterns based on subtle, not routinely measured, differences. For example, pauses may represent complete quiescence (Fig. 4F) or an active pause consisting of short back and forth movements, with active head foraging, seen as rapid changes in shading at the top (Fig. 4E). Fig. 3 also contains several examples of pauses indicated by arrows: an almost complete pause in Fig. 3D and additional pauses varying in degree of quiescence in the other panels. Sensitivity of the bend progagation visualization tool is also demonstrated by the ability of this tool to identify anatomical details. Specifically, the dark band indicated by the arrow in Fig. 4A indicates a kink in the waveform that corresponds to the vulva region. The anatomy of this region is likely to affect tissue rigidity, thus producing this small kink. Importantly, subtle differences identified by the visualization tools can be used to classify mutants. For example, in –T animals we often see a pattern indicating irregular bend propagation during forward movement, which is not seen in N2 (compare Fig. 4D with 4B). This difference is not obvious when comparing earlier time points at which animals move much faster (compare Fig. 4C with 4A).

Characterizing the dynamic response to transfer

The image analysis presented here is initiated quickly (<0.5 min) after transferring a single animal, using a wire pick, to the plate used for imaging. In previous analysis we allowed animals to recover from this procedure for 10 min following transfer (Albeg et al., 2011). Here, however, we examined the behavioral response to what is likely to be an extremely noxious mechanical insult. As described above, visual tools show that this procedure is associated with a dynamic shift from roaming, in the first minutes following transfer, to dwelling as time progresses. In order to enable analysis of locomotion dynamics, our program generates several outputs describing locomotion dynamics, in addition to summaries of locomotion and posture properties from the entire movie. Using these outputs it is possible to analyze how locomotion properties change over time.

End-to-end displacement over short time segments (0.5 min) is a sensitive measure that integrates information on speed and on efficiency of movement (reversals will reduce end-to-end displacement). Analysis of such end-to-end displacement in N2 shows that initially it is relatively high, and declines slowly over several minutes to finally reach a variable and low steady-state level lasting until the end of our movies (20 min, Fig. 6A). The results of this analysis can be fitted by an exponential function having a $t_{1/2}$ (τ) of 3.29 min (R^2=0.935, 95% confidence interval 2.69:4.24, Fig. 6A). Difference in the end-to-end displacement during the first minute of analysis relative to the last minute of analysis is significant (P<0.01). Similar decreasing trends were shown for speed and for the fraction of time spent in forward movement, while an opposite (increasing) trend was seen for the fraction of time spent in

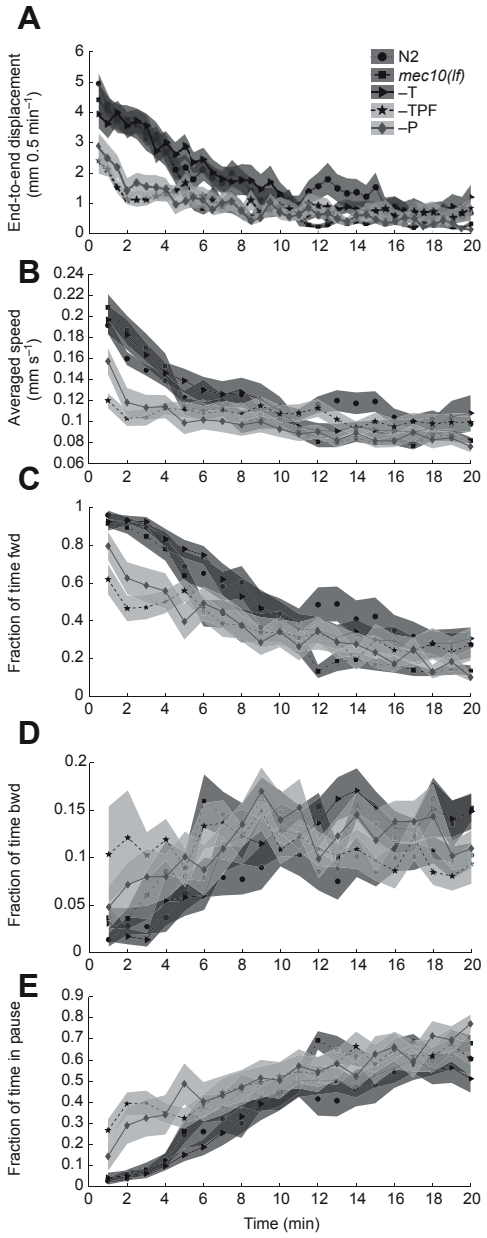

	a	*b*	τ[ln(2)/*b*]	*c*	R^2
N2	4.367 (3.944:4.789)	0.210 (0.163:0.258)	3.294	0.800 (0.583:1.017)	0.935
mec10(lf)	5.282* (4.828:5.736)	0.230 (0.187:0.272)	3.020	0.148* (–0.053:0.348)	0.951
–T	4.316 (3.959:4.674)	0.144 (0.106:0.182)	4.825	0.341 (–0.012:0.694)	0.942
–TPF	1.543* (1.219:1.866)	0.207 (0.105:0.310)	3.341	0.628 (0.458:0.799)	0.752
–P	2.519* (2.223:2.815)	0.235 (0.177:0.294)	2.944	0.398* (0.272:0.523)	0.914

	a	*b*	τ[ln(2)/*b*]	*c*	R^2
N2	0.107 (0.083:0.131)	0.294 (0.185:0.403)	2.358	0.106 (0.100:0.112)	0.909
mec10(lf)	0.173* (0.154:0.192)	0.249 (0.196:0.301)	2.788	0.079* (0.073:0.086)	0.972
–T	0.133 (0.115:0.151)	0.204 (0.141:0.267)	3.398	0.091* (0.082:0.100)	0.950
–TPF	–0.011* (–0.086:0.064)	–0.046 (–0.252:0.160)	–15.060†	0.124 (0.043:0.205)	0.499
–P	0.082 (0.063:0.102)	0.284 (0.170:0.398)	2.439	0.085* (0.080:0.090)	0.897

	a	*b*	τ[ln(2)/*b*]	*c*	R^2
N2	0.926 (0.801:1.051)	0.102 (0.057:0.148)	6.772	0.163 (0.001:0.324)	0.959
mec10(lf)	1.114 (1.002:1.227)	0.134 (0.088:0.180)	5.170	0.027 (–0.093:0.148)	0.963
–T	1.030 (0.885:1.175)	0.104 (0.056:0.153)	6.638	0.102 (–0.085:0.289)	0.953
–TPF	0.465* (0.322:0.608)	0.094 (0.005:0.182)	7.390	0.162 (–0.022:0.347)	0.856
–P	0.721 (0.609:0.834)	0.114 (0.053:0.175)	6.093	0.090 (–0.051:0.231)	0.930

	a	*b*	τ[ln(2)/*b*]	*c*	R^2
N2	–0.120 (–0.147:–0.092)	0.213 (0.107:0.320)	3.250	0.103 (0.091:0.115)	0.874
mec10(lf)	–0.173* (–0.250:–0.096)	0.318 (0.096:0.540)	2.179	0.144 (0.127:0.161)	0.732
–T	–0.191* (–0.228:–0.154)	0.143 (0.054:0.232)	4.843	0.167 (0.131:0.202)	0.876
–TPF	–0.001* (–0.006:0.004)	–0.205 (–0.609:0.200)	–3.385†	0.119 (0.100:0.138)	0.316
–P	–0.118 (–0.183:–0.053)	0.290 (0.023:0.557)	2.390	0.132 (0.115:0.149)	0.620

	a	*b*	τ[ln(2)/*b*]	*c*	R^2
N2	–0.841 (–1.005:–0.678)	0.082 (0.039:0.125)	8.445	0.769 (0.564:0.974)	0.960
mec10(lf)	–0.926 (–1.049:–0.803)	0.114 (0.062:0.167)	6.058	0.793 (0.640:0.946)	0.948
–T	–0.832 (–0.983:–0.681)	0.094 (0.042:0.147)	7.367	0.723 (0.528:0.918)	0.944
–TPF	–0.618 (–1.052:–0.184)	0.053 (–0.017:0.123)	13.034	0.876 (0.392:1.361)	0.895
–P	–0.720 (–1.029:–0.412)	0.067 (0.003:0.131)	10.394	0.894 (0.529:1.259)	0.913

Fig. 6. Quantitative analysis of movement dynamics. Analysis of wild-type animals (N2, *N*=14), animals lacking all body mechanosensors (–TPF, *N*=13), animals lacking PVD (–P, *N*=10), animals lacking touch receptor neurons (–T, *N*=13) and *mec-10(lf)* mutants (*N*=11). Left panels show how locomotion properties change with time (standard error interval is shaded) and right panels show values derived from fitting the data with an exponential function $f(x)=ae^{-bx}+c$ [*a* and *c* are in the same units as the *y*-axis on the left, *x* and ln2/*b* (τ) are in minutes]. The 95% confidence interval is given below each number. (A) End-to-end displacement measured for 0.5 min segments. (B) Speed (averaged over 1 min). (C) Fraction of time in forward movement. (D) Fraction of time in backward movement. (E) Fraction of time in pause. Asterisks indicate a significant difference relative to N2 ($P<0.05$, based on lack of overlap between 95% confidence intervals calculated using Matlab, Trust-Region algorithm). †Half life value is irrelevant as this data set does not fit the exponential function, low R^2.

backward movement and for the fraction of time spent in pause (Fig. 6). The frequency of reversals also increases with time; however, reversal frequency is highly variable and, thus, was not further analyzed. The strongest effect seen in this analysis is the suppression of pauses (a >20-fold effect, last minute relative to first minute). Previous analysis of the effects of noxious mechanical stimuli on locomotion showed a shorter, 100 s effect that was limited to suppression of reversals (Zhao et al., 2003). Differences between our data and previously reported data are likely to be a result of the higher sensitivity of our analysis, but may also represent differences in the assay conditions. Notably, both the previously published results and our results were obtained in the presence of food and thus are not confounded by the effects of food withdrawal (Zhao et al., 2003).

The dynamics of the response to transfer, shown in Fig. 6, reflect three factors: the starting point (locomotion immediately following transfer), the rate at which the response decays with time, and the end-point, likely to reflect steady-state behavior. To enable comparison between different strains we needed to characterize each of these factors. For this we fitted the results to an exponential function or to a linear function. In the exponential function $f(x)=ae^{-bx}+c$, *a* is the difference between the start point (time zero) and end point of the function (an estimate of the magnitude of the response to transfer), ln2/*b* is τ ($t_{1/2}$, half-life of the response) and *c* gives the end point, an estimate of steady-state behavior (basal locomotion). The resulting values are shown on the right side of Fig. 6. We do not show values derived from fitting data to linear functions as these functions show lower fits (R^2). Examples of fitted curves are shown in Fig. 7.

Previous work and the results shown in Fig. 3 (compare Fig. 3A with 3B) suggest a role for body mechanosensors in the response to transfer; evidence for this comes from analysis of *mec-3(lf)* mutants that are defective for differentiation of all 10 body mechanosensors and from analysis of animals in which all 10 cells degenerate (Zhao et al., 2003) (Fig. 3). To further examine which specific neurons and molecular mechanisms are required for this effect we analyzed previously described strains in which all or some of these neurons degenerate and a *mec-10(lf)* strain lacking the

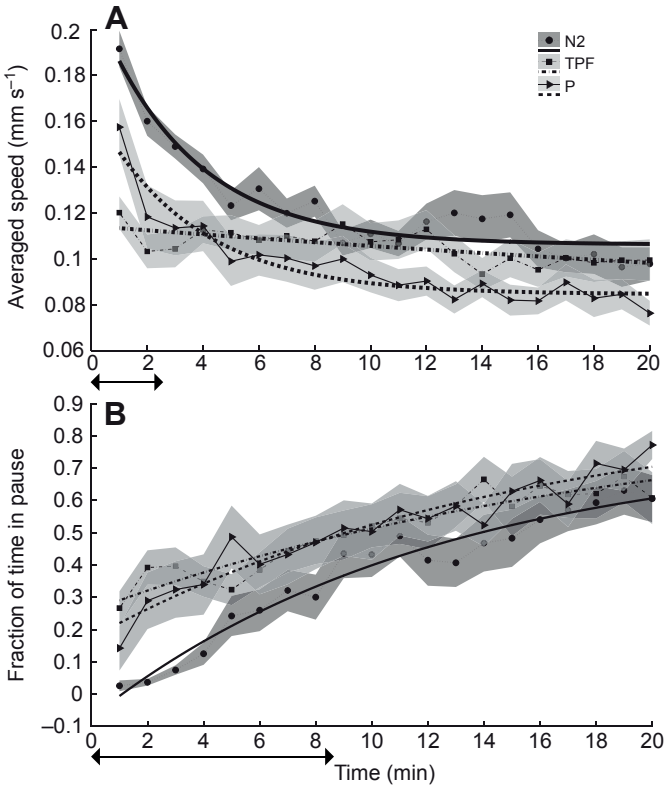

Fig. 7. Dynamics of speed and pause frequency are altered in –P and –TPF animals. Examples from data in Fig. 6 are shown with the addition of a fitted curve (thick lines) using an exponential function $f(x)=ae^{-bx}+c$. (A) Speed. (B) Fraction of time in pause. Only three strains are shown: wild-type animals (N2, N=14), animals lacking all body mechanosensors (–TPF, N=13) and animals lacking PVD (–P, N=10). Half-life estimates for N2 are indicated by arrows.

proposed PVD mechanosensory channel (Albeg et al., 2011; Chatzigeorgiou et al., 2010). The following results clearly show that eliminating all body mechanosensors eliminates or greatly reduces the effects of transfer on locomotion. First, b for speed of animals lacking all body mechanosensors (–TPF) is very small (Fig. 6) and therefore data on speed can also be fitted by a straight line with a slope of –0.0008 (95% confidence intervals –0.0012:–0.0004, R^2=0.49). Second, effects of transfer on other locomotion features of –TPF animals, as measured by a, are significantly reduced relative to N2 (Fig. 6). We note that although fits for N2 are excellent (R^2>0.85) fits for –TPF animals are always lower, sometimes much lower, when compared to N2. This difference between N2 and –TPF serves as additional evidence for effects of mechanosensory neurons on the behavioral response to transfer (Fig. 6). Interestingly, our results also show that PVD has a significant role in the response to transfer; in its absence, a of end-to-end displacement is significantly reduced relative to N2. Touch receptors, however, contribute little to this response, and in their absence a is not reduced and is even sometimes increased (fraction of time in backward movement). Thus, differences in the response (a) between animals lacking all body mechanosensors and those lacking only PVD can be attributed to FLPs. In addition, PVD is likely to express receptors for noxious mechanical stimuli in addition to *mec-10*, as was suggested previously (Li et al., 2011). *mec-10(lf)* was shown to eliminate the harsh touch response in PVDs, suggesting that *mec-10* is the harsh touch receptor in these neurons (Chatzigeorgiou et al., 2010). However, *mec-10(lf)* mutants behave differently from –P animals, even showing increased a relative to N2 for some measurements (Fig. 6).

One important outcome of fitting the response to transfer data with exponential functions is our ability to estimate half-lives for these responses. This analysis shows different half-lives for different locomotion features. Specifically, the half-life of the effect of transfer on speed for N2 is 2.35 min, and differs significantly from the half-live of the effect on pause, which is 8.4 min (Figs 6, 7). This correlates with results showing that in the absence of body mechanosensors (–TPF animals) effects on speed are eliminated while effects on pause are only reduced (a for N2 is –0.84 relative to –0.61 for –TPF for pauses) (Fig. 6). Thus, our results suggest that fraction of time pausing is governed by additional neurons, as yet unidentified, whose effects are longer lasting.

Previous analysis suggested effects of PVD and FLP on basal locomotion (Albeg et al., 2011). Those findings are supported by estimates of basal locomotion properties provided by c (Fig. 6). However, estimates given here are not identical to previously measured data, suggesting, for example, a significant effect of *mec-10* on basal locomotion properties. Importantly, the previous analysis characterized locomotion 10 min following transfer while the current analysis shows that some responses to transfer do not fully decay after 10 min. Validation of the new estimates for basal locomotion will, therefore, require analysis following longer intervals or a less intrusive means of transferring animals for analysis. Interestingly, values of c for –T animals suggest a significant reduction in basal speed. This reduction correlates with the irregular bend propagation seen in the same animals (Fig. 4D).

DISCUSSION

The analysis presented here relies on a new tool kit for analyzing *C. elegans* locomotion. Like previously described 'worm-tracking' tool kits, this tool kit enables high-resolution prolonged analysis of a single animal's locomotion (Baek et al., 2002; Cronin et al., 2005; Hoshi and Shingai, 2006; Tsibidis and Tavernarakis, 2007). It includes several improvements relative to previous tool kits. First, the worm-tracking hardware is cheaper and easier to assemble. Moreover, tracking is performed by moving the camera and not the stage, thus reducing mechanical perturbation that may affect behavior. Second, analysis of locomotion and posture properties is performed separately for different locomotion patterns (forward, backward, pause and omegas). This feature increases the sensitivity of the analysis and facilitates interpretation of the results. Last, this analysis produces several visual and frame-by-frame data outputs that enable identification and detailed analysis of locomotion and posture dynamics. Many of the analysis features of this tool kit were previously described (Albeg et al., 2011). However, they are now combined with the 'worm-tracking' hardware to enable higher resolution and prolonged analysis.

Using this tool kit we examined the roles of genes and neurons known to function in mechanosensation. The results of this analysis support some of our previous findings, add new functions to previously characterized neurons, and enable better interpretation of previous results. Specifically, this analysis produced the following novel findings. (1) There is a bias in the movement direction of animals lacking the six touch receptors. (2) The behavioral response to transfer is prolonged, lasting several minutes. (3) Some of the neurons participating in the response to transfer were identified and a non-redundant role for PVD in this response was revealed.

The six touch receptor neurons are a set of well-characterized neurons mediating the response to low threshold mechanical stimuli

to the nematode's body (Chalfie and Sulston, 1981; Chalfie et al., 1985; Wicks and Rankin, 1995). Mutations interfering with the function of these neurons were also shown to affect locomotion within a structured environment, to control forward thrashing frequency in liquid, and to control speed and wave propagation (Korta et al., 2007; Lebois et al., 2012; Park et al., 2008). Here, we show for the first time that touch receptor neurons function to regulate direction bias. Our results suggest that during forward movement wild-type animals have a ventral bias in movement direction, possibly as a result of asymmetric innervations, as previously shown for backward movement (Gray et al., 2005). We show that in the absence of touch receptor neurons this bias is enhanced. Thus, we suggest that touch receptor neurons also have a role in regulating locomotion in the absence of obvious extrinsic inputs and thus may sense intrinsic signals such as subtle differences in posture.

Previous studies looking at the response to noxious mechanical stimuli applied to the body focused on the response to prodding with a wire pick (Albeg et al., 2011; Chatzigeorgiou et al., 2010; Li et al., 2011; Way and Chalfie, 1989; Zhao et al., 2003). These studies identified PVD and touch receptor neurons as mechanosensors functioning redundantly to mediate the response to harsh touch. Our work focuses on the behavioral response to transfer with a wire pick. This behavioral response was previously characterized in a single study (Zhao et al., 2003). Like the response to harsh touch this behavior requires the activity of body mechanosensors and thus is likely to represent the response to a particularly noxious mechanical stimulation. We show that in wild-type animals this response, unlike the transient response to harsh touch or to optogenetic stimulation of PVD, is a sustained response (half-life of 2–8 min relative to five head swings for anterior prodding, i.e. several seconds, or ~5 s for brief optogenetic stimulation (Li et al., 2011; Husson et al., 2012). We also show that in this response, unlike in the harsh touch response, PVD has a non-redundant role. Moreover, touch receptor neurons that function redundantly with PVD in the harsh touch response have a minor role in the response to transfer.

Previous work suggested that PVD utilizes the DEG/ENaC channel MEC-10 as a mechanosensory channel (Chatzigeorgiou et al., 2010). This conclusion was disputed in later publications (Arnadóttir et al., 2011; Li et al., 2011). For example, results of electrophysiological recordings from PVD following harsh touch were unaffected by mutation of *mec-10* (Li et al., 2011). Similarly, our analysis shows that PVD-mediated responses to transfer are unaffected by mutation in *mec-10*. The conflicting results concerning the role of MEC-10 in PVD-mediated responses to high-threshold mechanical stimuli can be explained by differences in intensity of the applied stimulus or by differences in the assay used to examine the response. Based on these conflicting results we suggest that PVD, like *Drosophila* DA-IV nociceptors, employs more than one mechanosensor (Kim et al., 2012).

The response to high-threshold mechanical stimulation (prodding with a wire pick) is either forward movement or reversals (Li et al., 2011; Way and Chalfie, 1989). Careful analysis showed that the response to such prodding depends on the body region receiving the stimulus; prodding the anterior region led to reversals and prodding to the posterior region led to forward movement (Li et al., 2011). Similar conclusions were obtained from optogenetic analysis (Husson et al., 2012). Thus, the behavioral response to mechanical inputs depends on the identity of the responding sensory neurons. Specifically, FLPs, innervating the head, and not PVDs, innervating the body, are required for the response to anterior stimulation and thus for reversals (Li et al., 2011). Transfer with a wire pick, unlike prodding with a wire pick, appears to activate both anterior and posterior mechanosensors. This difference in the stimulation protocol, combined with detailed and prolonged analysis of multiple locomotion properties, shows that body mechanosensors can function together to produce a response that appears to be more than the sum of the responses elicited by activating each neuron individually.

Our analysis, while showing the importance of PVDs and FLPs in the response to transfer, also supports the involvement of additional neurons, as animals lacking PVDs, FLPs and touch receptor neurons (–TPF animals) still show many alterations in movement properties following transfer. Thus, our results are in agreement with previous results suggesting the involvement of additional neurons in this behavior (Zhao et al., 2003). Indeed, even the response to harsh touch appears to require additional cells (Li et al., 2011). Importantly, we show that transfer affects multiple locomotion properties having different half-lives and depending on the activity of overlapping but not identical sets of neurons. Specifically, the effects of transfer on pauses are much more prolonged than the effects on speed. And while speed is strongly affected by PVD and FLP, pauses are only weakly affected and are instead governed by a distinct yet unidentified set of neurons.

Some of the results obtained in this study reproduce previous results (Albeg et al., 2011), but the current more detailed analysis leads to interesting differences and to better understanding. In particular, some of the results have now been reinterpreted. For example, PVD and FLP were previously shown to affect locomotion. But this analysis was conducted 10 min after transfer, at which time the effects of transfer have not yet fully decayed. The current analysis shows that differences between strains lacking PVD and FLP and wild-type animals can be partly attributed to the long-lasting effects of transfer to a new plate. Importantly, the current analysis also identifies phenotypes that were previously masked by the effects of transfer. For example, we now show a reduced 'steady-state' speed of *mec-10(lf)* mutants and animals lacking touch receptor neurons (–T). The effects of transfer on the speed of these strains are greater than effects on wild-type animals, masking their 'steady-state' phenotype. We conclude that characterization of behavioral dynamics enables better interpretation and more sensitive detection of behavioral phenotypes.

ACKNOWLEDGEMENTS

We thank the Caenorhabditis Genetics Center for strains.

FUNDING

This research received no specific grant from any funding agency in the public, commercial, or not-for-profit sectors.

REFERENCES

Albeg, A., Smith, C. J., Chatzigeorgiou, M., Feitelson, D. G., Hall, D. H., Schafer, W. R., Miller, D. M. and Treinin, M. (2011). *C. elegans* multi-dendritic sensory neurons: morphology and function. *Mol. Cell. Neurosci.* **46**, 308-317.

Arnadóttir, J., O'Hagan, R., Chen, Y., Goodman, M. B. and Chalfie, M. (2011). The DEG/ENaC protein MEC-10 regulates the transduction channel complex in *Caenorhabditis elegans* touch receptor neurons. *J. Neurosci.* **31**, 12695-12704.

Baek, J. H., Cosman, P., Feng, Z., Silver, J. and Schafer, W. R. (2002). Using machine vision to analyze and classify *Caenorhabditis elegans* behavioral phenotypes quantitatively. *J. Neurosci. Methods* **118**, 9-21.

Ben Arous, J., Laffont, S. and Chatenay, D. (2009). Molecular and sensory basis of a food related two-state behavior in *C. elegans*. *PLoS ONE* **4**, e7584.

Chalfie, M. and Sulston, J. (1981). Developmental genetics of the mechanosensory neurons of *Caenorhabditis elegans*. *Dev. Biol.* **82**, 358-370.

Chalfie, M., Sulston, J. E., White, J. G., Southgate, E., Thomson, J. N. and Brenner, S. (1985). The neuronal circuit for touch sensitivity in *Caenorhabditis elegans*. *J. Neurosci.* **5**, 956-964.

Chatzigeorgiou, M., Yoo, S., Watson, J. D., Lee, W.-H., Spencer, W. C., Kindt, K. S., Hwang, S. W., Miller, D. M., Treinin, M., Driscoll, M. et al. (2010). Specific roles for DEG/ENaC and TRP channels in touch and thermosensation in *C. elegans* nociceptors. *Nat. Neurosci.* **13**, 861-868.

Croll, N. A. (1975). Components and patterns in the behaviour of the nematode *Caenorhabditis elegans*. *J. Zool.* **176**, 159-176.
Cronin, C. J., Mendel, J. E., Mukhtar, S., Kim, Y. M., Stirbl, R. C., Bruck, J. and Sternberg, P. W. (2005). An automated system for measuring parameters of nematode sinusoidal movement. *BMC Genet.* **6**, 5.
Driscoll, M. and Chalfie, M. (1991). The *mec-4* gene is a member of a family of *Caenorhabditis elegans* genes that can mutate to induce neuronal degeneration. *Nature* **349**, 588-593.
Geng, W., Cosman, P., Berry, C. C., Feng, Z. and Schafer, W. R. (2004). Automatic tracking, feature extraction and classification of *C. elegans* phenotypes. *IEEE Trans. Biomed. Eng.* **51**, 1811-1820.
Gray, J. M., Hill, J. J. and Bargmann, C. I. (2005). A circuit for navigation in *Caenorhabditis elegans*. *Proc. Natl. Acad. Sci. USA* **102**, 3184-3191.
Hoshi, K. and Shingai, R. (2006). Computer-driven automatic identification of locomotion states in *Caenorhabditis elegans*. *J. Neurosci. Methods* **157**, 355-363.
Husson, S. J., Steuer Costa, W., Wabnig, S., Stirman, J. N., Watson, J. D., Spencer, W. C., Akerboom, J., Looger, L. L., Treinin, M., Miller, D. M. et al. (2012). Optogenetic analysis of a nociceptor neuron and network reveals modulatory ion channels acting downstream of nociceptive sensors. *Curr. Biol.* **22**, 743-752.
Kaplan, J. M. and Horvitz, H. R. (1993). A dual mechanosensory and chemosensory neuron in *Caenorhabditis elegans*. *Proc. Natl. Acad. Sci. USA* **90**, 2227-2231.
Kim, S. E., Coste, B., Chadha, A., Cook, B. and Patapoutian, A. (2012). The role of *Drosophila* piezo in mechanical nociception. *Nature* **483**, 209-212.
Korta, J., Clark, D. A., Gabel, C. V., Mahadevan, L. and Samuel, A. D. (2007). Mechanosensation and mechanical load modulate the locomotory gait of swimming *C. elegans*. *J. Exp. Biol.* **210**, 2383-2389.
Lebois, F., Sauvage, P., Py, C., Cardoso, O., Ladoux, B., Hersen, P. and Di Meglio, J. (2012). Locomotion control of *Caenorhabditis elegans* through confinement. *Biophys. J.* **102**, 2791-2798.
Li, W., Kang, L., Piggott, B. J., Feng, Z. and Xu, X. Z. (2011). The neural circuits and sensory channels mediating harsh touch sensation in *Caenorhabditis elegans*. *Nat. Commun.* **2**, 315.
Park, S., Hwang, H., Nam, S. W., Martinez, F., Austin, R. H. and Ryu, W. S. (2008). Enhanced *Caenorhabditis elegans* locomotion in a structured microfluidic environment. *PLoS ONE* **3**, e2550.
Stephens, G. J., Johnson-Kerner, B., Bialek, W. and Ryu, W. S. (2010). From modes to movement in the behavior of *Caenorhabditis elegans*. *PLoS ONE* **16**, e13914.
Tsalik, E. L. and Hobert, O. (2003). Functional mapping of neurons that control locomotory behavior in *Caenorhabditis elegans*. *J. Neurobiol.* **56**, 178-197.
Tsibidis, G. D. and Tavernarakis, N. (2007). Nemo: a computational tool for analyzing nematode locomotion. *BMC Neurosci.* **8**, 86.
Von Stetina, S. E., Treinin, M. and Miller, D. M. (2006). The motor circuit. *Int. Rev. Neurobiol.* **69**, 125-167.
Wakabayashi, T., Kitagawa, I. and Shingai, R. (2004). Neurons regulating the duration of forward locomotion in *Caenorhabditis elegans*. *Neurosci. Res.* **50**, 199-216.
Way, J. C. and Chalfie, M. (1989). The *mec-3* gene of *Caenorhabditis elegans* requires its own product for maintained expression and is expressed in three neuronal cell types. *Genes Dev.* **3**, 1823-1833.
White, J. G., Southgate, E., Thomson, J. N. and Brenner, S. (1986). The structure of the nervous system of the nematode *Caenorhabditis elegans*. *Phil. Trans. R. Soc. B* **314**, 1-340.
Wicks, S. R. and Rankin, C. H. (1995). Integration of mechanosensory stimuli in *Caenorhabditis elegans*. *J. Neurosci.* **15**, 2434-2444.
Zhao, B., Khare, P., Feldman, L. and Dent, J. A. (2003). Reversal frequency in *Caenorhabditis elegans* represents an integrated response to the state of the animal and its environment. *J. Neurosci.* **23**, 5319-5328.